International Journal of Multiphase Flow 36 (2010) 406–422

Contents lists available at ScienceDirect

International Journal of Multiphase Flow

journal homepage: www.elsevier.com/locate/ijmulflow

Wake response of a stationary finite-sized particle in a turbulent channel flow

Lanying Zeng [a], S. Balachandar [b,*], Fady M. Najjar [c]

[a] Department of Physics, University of Illinois at Urbana-Champaign, Urbana, IL 61801, USA
[b] Department of Mechanical and Aerospace Engineering, University of Florida, Gainesville, FL 32611, USA
[c] Lawrence Livermore National Laboratory, Livermore, CA, USA

ARTICLE INFO

Article history:
Received 19 March 2009
Received in revised form 31 December 2009
Accepted 5 January 2010
Available online 11 January 2010

Keywords:
Turbulence modulation
Particle wake
Drag and lift forces
Direct numerical simulation

ABSTRACT

Here we consider the effect of a finite-sized stationary particle in a channel flow of modest turbulence at $Re_\tau = 178.12$. The size of particle is varied such that the particle Reynolds number ranges from about 40 to 450. The location of the particle is chosen to be either in the buffer layer ($y_{p+} = 17.81$) or at the channel center. Fully resolved direct numerical simulations of the turbulent channel flow around the particles is performed. Here the ambient turbulence intensity relative to the mean velocity seen by the particle is large ($I = 23.16\%$) in the buffer region, while it is substantially lower ($I = 4.09\%$) at the channel center. We present results on turbulence modulation due to the particle in terms of wake dynamics and vortex shedding.

1. Introduction

Modulation of the carrier-phase by suspended particles is an important aspect of dispersed multiphase flows. The experiments by Tsuji et al. (1984) in a turbulent pipe flow are good examples to illustrate the effect of particles on the flow. They measured the mean turbulent velocity profile across the pipe with and without the particles. Their measurements showed that with $d = 500$ μm particles the mean velocity distribution can be greatly altered. The peak velocity progressively shifted from the pipe center to somewhere halfway between the wall and the center of the pipe as the mass leading increased from 0 to 3.5. In contrast, with the larger particles of $d = 1$ mm the change in the mean velocity profile for the same level of mass loading is not nearly as dramatic.

It has also been well established that the introduction of particles can augment or suppress carrier-phase turbulence. In a dilute suspension there are several mechanisms that contribute to turbulence modulation. On one hand the particles acts to dampen carrier-phase turbulence. This reduction is due to: (a) the enhanced density (inertia) of the particle-laden flow, (b) increased dissipation arising from particle drag, and (c) the enhanced effective viscosity of the particle-laden fluid. On the other hand, particles can contribute to turbulence enhancement in two different ways: (a) the wake dynamics behind the particles, either in response to ambient oncoming turbulence or due to self-induced vortex shedding in case of larger particles, contribute to enhanced velocity fluctuation and (b) density variation arising from particle concentration fluctuation can contribute to buoyancy-induced instabilities and act as source of turbulence.

The length scale at which these different turbulence augmentation and suppression mechanisms are active varies. For example, wake dynamics and vortex shedding contribute to velocity fluctuations at length scales comparable to the particle size. In contrast, turbulence augmentation due to buoyancy-induced instability will be at length scales of concentration fluctuation, which are typically much larger than the particle size. Thus, when the unladen and laden turbulence energy spectra are compared, augmentation and suppression can be simultaneously observed over different range of scales. The overall effect of suspended particles on carrier-phase turbulence, measured in terms of rms velocity fluctuation, can either be net increase or decrease depending on the relative strength of the different mechanisms.

Based on a collection of experimental measurements Crowe et al. (1998) suggested that turbulence modulation is dictated by the ratio of particle diameter to the characteristic size of the energy containing eddies. If this ratio is greater than 0.1, turbulence is augmented and otherwise suppressed (see also Pan and Banerjee, 1997). On the other hand Elghobashi and Truesdell (1993) observed turbulence enhancement even for particles of diameter comparable to the Kolmogorov scale of turbulence. Thus, a simple criterion based only on a single parameter may not be adequate to accurately predict turbulence modulation with universal applicability.

Here we will focus on the mechanism of turbulence modulation by wake oscillation and vortex shedding. Hetsroni (1989) argued that the vortex shedding process is responsible for turbulence augmentation and therefore suggested $Re > 400$ to be the criterion for

* Corresponding author. Tel.: +1 352 392 0961; fax: +1 352 392 7303.
E-mail address: bala1s@ufl.edu (S. Balachandar).

0301-9322/$ - see front matter © 2010 Elsevier Ltd. All rights reserved.
doi:10.1016/j.ijmultiphaseflow.2010.01.001

turbulence enhancement. Mittal (2000) and Bagchi and Balachandar (2004) have however observed vortex shedding process to initiate at even lower *Re*, triggered by freestream turbulence. Their results also suggest that vortex shedding is not the only mechanism for turbulence enhancement, wake oscillation in response to freestream turbulence is another mechanism. However, enhancement by wake oscillation is smaller than by vortex shedding. At lower levels of freestream turbulence, vortex shedding enhances the fluctuation turbulent energy significantly. At higher levels of freestream turbulence, the effect of particles is to only marginally enhance, or even suppress, turbulence. Wu and Faeth (1994b) experimentally studied the effect of freestream turbulence on particle wake and vortex shedding in a homogeneous pipe flow. They suggested that the turbulent wakes behave like self-preserving laminar wakes. Further, by varying the level of freestream turbulence, they concluded that at intermediate particle Reynolds numbers the increase in cross-stream velocity fluctuations is reduced with increasing turbulence intensity. The numerical results of Bagchi and Balachandar (2003, 2004) for an isolated finite-sized particle in an isotropic turbulence showed good agreement with the data of Wu and Faeth (1994a,b). Recent computational and experimental works by Eaton and co-workers (Burton and Eaton, 2005; Hwang and Eaton, 2006) have also considered the interaction of isotropic turbulence with particles.

Of particular interest here is the effect of particle in the context of wall turbulence. Several experiments have addressed the problem of particulate wall-bounded flows (Rashidi et al., 1990; Young and Hanratty, 1991; Fessler et al., 1994; Kaftori et al., 1995a,b; Suzuki et al., 2000; Caraman et al., 2003). These efforts have generally been at the level of many particles. Further the computational efforts have generally limited to small particles and employed the point particle assumption. The works of Pan and Banerjee (1997), Kajishima et al. (2001) and Uhlmann (2008) considered a distribution of finite-sized particles in wall turbulence.

Here we consider a single isolated finite-sized stationary particle placed in a turbulent channel flow. The size of the particle relative to the channel, or equivalently the particle Reynolds number, will be varied and two different particle locations within the channel, one in the buffer layer and the other in the channel center plane will be considered. The present report follows our earlier work (Zeng et al., 2008) which focused attention exclusively on the effect of the ambient turbulent flow on the particle and the resulting time-dependent drag and lift forces and our ability to predict them with existing correlations. In the present work we will focus attention on the back effect of the particle on the flow.

The turbulence statistics in the particle wake will be compared with corresponding statistics in the undisturbed flow (in the absence of the particle). Particular attention will be paid to wake oscillation and self-induced vortex shedding in the wake and their contribution to total and fluctuation kinetic energy. The anisotropic nature of velocity fluctuation in the wake will be quantified. The effect of the particle size (or particle Reynolds number) and particle location on turbulence modulation in the wake will be considered. For the cases of particle location within the buffer region the interaction with the wall will be of interest. For the cases where the particle is at the channel center, the recent work by Merle et al. (2005) is of relevance, since they considered turbulent pipe flow over a stationary spherical bubble positioned along the axis of the pipe using large eddy simulation. Also along the channel center the turbulence encountered by the particle is likely to be nearly isotropic.

2. Problem description

In this work we consider a fully developed turbulent channel flow between two infinite smooth parallel plates, with the Reynolds number (based on channel half-height, H and friction velocity u_τ) chosen to be $Re_\tau = Hu_\tau/\nu = 178.12$, where ν is the kinematic viscosity of the fluid. A rigid stationary spherical particle of diameter, d, is located within the channel at a distance y_p from the bottom wall. The diameter of the particle and the distance from the wall in wall units are defined as $d_+ = du_\tau/\nu$ and $y_{p+} = y_p u_\tau/\nu$, respectively. In this study, we consider a range of particle diameters varying from about 3.5 to 25 wall units. The particle is placed either within the buffer region at a distance $y_{p+} = 17.81$ from the bottom wall or along the channel center at $y_{p+} = 178.12$. When placed in the buffer layer, the smallest particle is entirely within the buffer region, while the largest particle extends almost into the viscous sublayer. For the largest particle ($d+ = 24.94$), the gap between the bottom of the particle and the bottom wall is only 5.34 wall units.

Table 1
Parameters for the study of particle wake response.

Case	y_{p+}	$I = u_{\rm rms}/\langle u\rangle$ (%)	d_+	d/η	Re	y_p/d
1	17.81	23.16	3.56	2.0	42	5.0
2			10.69	6.1	125	1.66
3			17.81	10.2	210	1.0
4			24.94	14.3	295	0.72
5	178.12	4.09	17.81	4.8	325	
6			24.94	6.7	455	

The details of the six cases considered are shown in Table 1. Since the statistics is inhomogeneous along the wall-normal direction, the Kolmogorov scale (η) increases from near the wall to the channel center. In the buffer region at $y_{p+} = 17.81$, d/η varies from about 2.0 to 14.3, while at the channel center this ratio for cases 5 and 6 is 4.8 and 6.7. The instantaneous relative velocity is simply the local fluid velocity and time-averaged particle Reynolds number is given by $Re = \langle\langle u_+(y_{p+})\rangle\rangle d_+$, where the double angle brackets represent an average over both time and horizontal plane. The mean particle Reynolds number for cases 1–4 at $y_{p+} = 17.81$ varies from 42 to 295. At the channel center the particle Reynolds number is larger and is equal to 325 and 455 for cases 5 and 6. Furthermore, the ratio of ambient rms velocity fluctuation ($u_{\rm rms}$) to the mean relative velocity is only a function of particle location and the ratio is 23.16% and 4.09% at $y_{p+} = 17.81$ and $y_{p+} = 178.12$, respectively. Thus, the particle in the buffer layer experiences intense turbulence, while at the centerline the relative intensity of the oncoming turbulence is weak.

The present simulations employ spectral element methodology and an existing SEM code (Nek5000) has been used. The computational domain is partitioned into hexahedral elements and within each element, velocity and pressure are represented in local Cartesian coordinates by tensor-product Lagrange polynomials of degree N and $N-2$, respectively. Time stepping is based on a semi-implicit splitting scheme that, with correct treatment of the incompressibility constraint, allows high-order temporal accuracy. Along the spanwise (z) direction, periodic boundary conditions are employed and the spanwise extent of the computational domain is $4\pi/3$ times the half-channel height. The streamwise (x) extent of the computational domain is 2.4 times the half-channel height. Unlike standard turbulent channel-flow simulations that employ a longer streawise domain with periodic boundary conditions, here we employ a shorter streamwise domain with a fully developed turbulent channel flow applied as inflow at the upstream inlet end of the computational domain. A simple convective outflow boundary condition is applied at the other end. The reason for the inflow–outflow simulation is that a periodic boundary condition along the streamwise direction is not possible with the particle in the interior. The turbulent inflow was computed from a companion turbulent channel-flow simulation. The wall turbulence was fully sustained in the inflow–outflow simulation and the statistics computed without the particle was in complete agreement with the periodic turbulent channel flow results (see Zeng et al., 2008).

The results reported here employ 3400 spectral elements with each element resolved by $11 \times 11 \times 11$ Legendre–Gauss–Lobatto points. The present inflow–outflow simulations thus employ 3.4 million points, which can be compared with the 2.1 million points used for the standard $(128)^3$ streamwise-periodic turbulent channel-flow simulation. Because of the shorter streamwise domain, the effective resolution of the inflow–outflow simulation is about eight times finer than the corresponding channel-flow simulation. The cross-sectional area of the largest particle under consideration is only 0.18% of the total channel cross-section. For the smallest particle, the cross-sectional area is two orders of magnitude smaller and thus in all cases considered, the blockage effect due to the particle is negligible. For additional details of the numerical methodology employed in these simulations, and adequacy of spatial and temporal resolution refer to Zeng et al. (2008).

Here the primary objective is to present results on the effect of turbulence on particle wake and vortex shedding, and on the modulation of ambient turbulence by the particle. Therefore, frequent comparison between the turbulent flow with and without the particle will be made. For the sake of simplicity, the term 'undisturbed' will be used to refer to the turbulence simulation without the particle. Furthermore, for each case in Table 1, we also performed a companion simulation at the same mean particle Reynolds number, *Re*, and distance from the wall y_{p+}, but in a non-turbulent laminar wall-bounded flow. For the cases of a particle placed at the channel center (cases 5 and 6), the particle could be considered to be in a quasi-isotropic flow, since the particle is far from both the walls. These cases can also be compared with those for a particle immersed in an unbounded uniform cross flow. Thus, together with the six companion laminar simulations, a total of 12 simulations will be discussed below.

3. Results and discussion

3.1. Mean wake

The mean streamwise velocity, averaged over time, along the *x*-axis is shown in Fig. 1 for all the six cases (here $x = 0$ corresponds to the center of the particle). Due to differences in the sphere size between the six cases, the downstream distance is scaled by the radius of the sphere ($a = d/2$). The mean streamwise velocity $\langle u \rangle$ is measured along the particle centerline passing through the sphere center. With the particle present, the turbulence statistics in the wake is inhomogeneous along all three directions, and this is in contrast to a turbulent channel flow without the particle, where the statistics is homogeneous along both the streamwise and spanwise directions. As a result, with the particle present the mean is defined only in terms of time average. Here $\langle u_0 \rangle$ indicates the 'undisturbed' mean streamwise velocity (i.e. without the particle) at the same particle location in a turbulent channel flow. Fig. 1a and b are for the cases of the buffer region and the channel center, respectively. The magnitudes of the peak reverse flow along the particle centerline are quite different in the buffer region compared to the channel center. For the buffer region cases, the magnitude is less than 10%, while it is around 25% for the channel center cases, as shown in Table 2.

Table 2
Magnitude of peak reverse flow and wake length.

Case	Along particle centerline		Maximum in wake region	
	$\langle u \rangle / \langle u_0 \rangle$ (%)	Le/a	$\langle u \rangle / \langle u_0 \rangle$ (%)	Le/a
1	1.55	0.61	1.55	0.61
2	9.24	1.26	11.00	1.50
3	5.05	0.88	13.97	1.56
4	0.56	0.41	13.15	1.45
5	24.89	2.57	24.89	2.57
6	26.87	2.58	26.87	2.58

The level of turbulent fluctuation in a channel flow varies across the channel, with its peak in the buffer region and somewhat lower at the channel center. In contrast, the mean streamwise velocity steadily increases towards the channel center. For the present case of a stationary particle, the ratio of rms turbulent fluctuation to mean relative velocity was presented in Table 1. The difference in relative turbulence level has a substantial impact. The difference in the magnitudes of the peak reverse flow for particles in the buffer region and channel center, shown in Table 2, is one of the consequences. As we will discuss later, the turbulence level has a strong impact on particle wake oscillation, and on the onset of vortex shedding. With a higher turbulence level the flow is more chaotic, and thus turbulence modulation by the particle is relatively weaker.

As noticed in Table 2, the behaviors of both the peak reverse flow and the wake length (*Le*), as measured in terms of the zero crossing of the streamwise velocity along the particle centerline, show a similar non-monotonic trend in the buffer region cases (cases 1–4). In the context of a spherical particle in a uniform flow, it has been well established that the wake length monotonically increases with Reynolds number (Johnson and Patel, 1999; Rimon and Cheng, 1969; Taneda, 1956). For example, the wake length measured from the base of the sphere to the reattachment point along the particle cen-

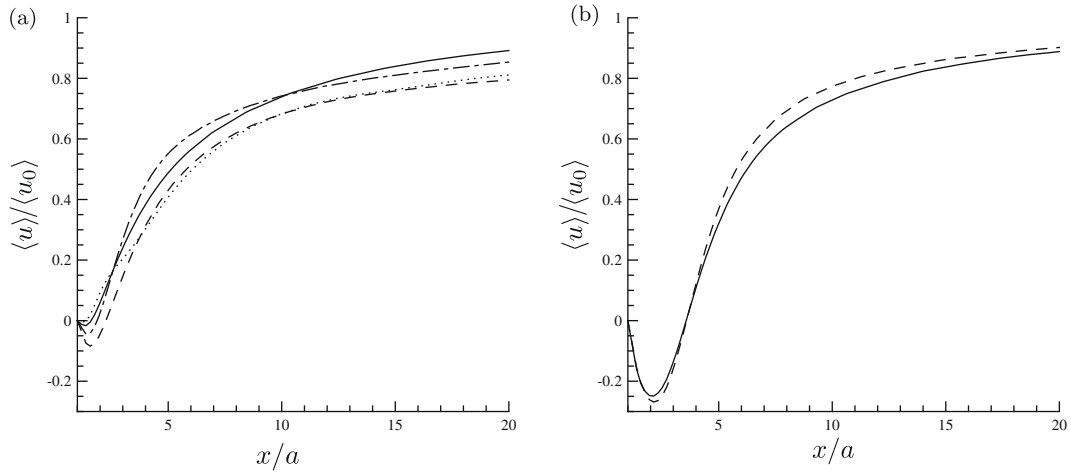

Fig. 1. Mean streamwise velocity along streamwise direction. (a) In the buffer region $y_{p+} = 17.81$. —: Case 1, - - - : Case 2. — · —: Case 3, ···: Case 4. (b) At the channel center $y_{p+} = 178.12$. —: Case 5, - - -: Case 6.

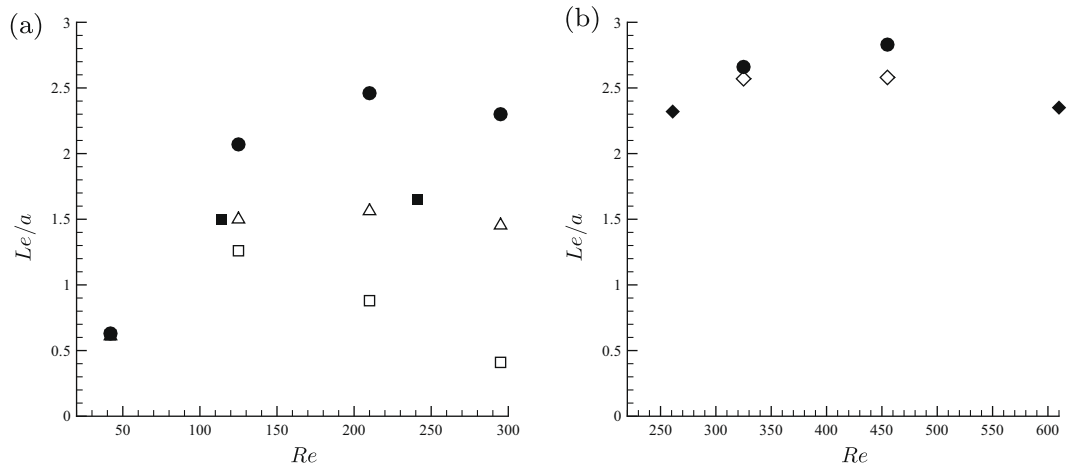

Fig. 2. The length *Le* of mean circulation region. (a) In the buffer region $y_{p+} = 17.81$. (b) At the channel center $y_{p+} = 178.12$. □: Present, turbulent flow in the buffer region measured along the particle centerline. △: Present, turbulent flow in the buffer region measured with the maximum distance between the zero streamwise velocity contour and the sphere surface. •: Present, companion laminar flow measured along the particle centerline. ■: Isotropic turbulence with $I = 25\%$ by Bagchi and Balachandar (2004). ◇: Present, turbulent flow at the channel center. ◆: Isotropic turbulence with $I = 10\%$ by Bagchi and Balachandar (2004).

terline increases from about $0.7a$ at $Re = 40$ to about $2.2a$ at $Re = 200$. As can be observed in Table 2 the wake length in the present simulations, as measured along the particle centerline, and its non-monotonic variation with *Re* shows a different behavior. This non-monotonic variation is the consequence of increasing particle Reynolds number combined with decreasing gap between the particle and the wall and the turbulent nature of the ambient flow.

Also shown in Table 2 are magnitude of peak reverse flow and the true wake length. Here we are not restricted to measurement only along the particle centerline. The peak reverse flow is taken to be the maximum negative streamwise velocity anywhere in the wake and similarly the contour of zero streamwise velocity (as shown later in Fig. 4) is used to evaluate the true wake length. As can be seen from the table, when the tilting of the wake is accounted for, the peak reverse flow and wake length increases from case 1 to case 2 to case 3. With further increase in particle size, as will be seen below, vortex shedding becomes dominant and enhanced unsteadiness is observed in the particle wake. This contributes to a reduction in both the peak reverse flow and the wake length from case 3 to case 4. The onset of self-induced vortex shedding episodically occurs even in case 3, and this could explain the only modest increase from case 2. For the case of particle located at the channel center, the mean wake is nearly axisymmetric and the information along the particle centerline is sufficient for extracting peak reverse flow and the wake length.

In cases 5 and 6, since the particle is sufficiently far away from the wall, the larger particle offers bigger hindrance to the flow resulting in a higher magnitude and larger extent of reverse flow. With the same turbulent inflow, case 6 has a higher magnitude of peak reverse flow since the particle is larger. For the buffer region cases, the reasoning is not as simple as that at channel center because of the wall effect. As the particle is positioned closer to the wall, the wake tilts away from the wall, and thus the mean streamwise velocity measured along the streamwise centerline passing through the sphere center does not provide a good estimate of the reverse flow.

Regarding the wall effect, we may notice that in cases 1 and 2 the particle is at a larger relative distance from the wall and therefore, the wall does not exert substantial influence in these two cases. From case 1 to case 2, the magnitude of peak reverse flow shows an increasing trend, same as in cases 5–6. Therefore, we could discuss solely the effect of turbulence levels by comparing cases 1 and 2 for a high turbulence level ($I = 23.16\%$) and cases 5 and 6 for a low turbulence level ($I = 4.09\%$) excluding the wall effect.

Fig. 2 shows the mean wake lengths (open symbols) compared with those for the companion laminar flows. The results of Bagchi and Balachandar (2004) for a particle subjected to isotropic turbulence is also shown (filled symbols). Fig. 2a shows the buffer region results (cases 1–4). In case 1, since the Reynolds number is low and the particle is sufficiently far away from the wall, the wake length matches with that of the companion laminar flow. From case 1 to 2, the wake length increases as the wall has not come to play a significant role. The mean wake length for cases 2 and 3 ($I = 23.16\%$) measured along the tilted wake line (shown in △) show good agreement with Bagchi and Balachandar's result for $I = 25\%$. This good agreement is due to the similar turbulence intensity and Reynolds number. Case 4 shows a slight decreasing behavior.

The cases at the channel center (cases 5 and 6) are shown in Fig. 2b. As expected, without the wall effect, the wake length increases as particle Reynolds number increases, consistent with the results for the companion laminar flows and the isotropic turbulence. As noticed, the increase from case 5 to 6 is small as vortex shedding is present in both cases. A small increase in wake length with particle Reynolds number is also observed in isotropic turbulence. Note that the wake length of the current simulation is slightly higher than that of the isotropic turbulence. This is the effect of the turbulence intensity of the oncoming flow, which is quite low at the channel center ($I = 4.09\%$), while it was larger in the isotropic turbulence simulations of Bagchi and Balachandar (2004) ($I > 10\%$). Furthermore, the wake length in the companion laminar flow is longer than that in the turbulent simulations. This trend is consistent with the picture that the wake is not well mixed in the laminar flow and with increasing intensity of ambient turbulence, the level of fluctuation increases in the wake and contributes to a faster recovery in the wake.

As to the wake velocity recovery, vortex shedding plays an important role. Fig. 3a and b shows the mean streamwise velocity variation of cases 1–4 $y_{p+} = 17.81$) and cases 5 and 6 $y_{p+} = 178.12$), respectively. The plot is in terms of normalized velocity deficit and thus it starts at 1.0 on the particle ($x/a = 1$) and increases in the wake due to reverse flow. Farther downstream the deficit decreases. The decay rate is observed to be $(x/a)^{-1}$ for the near-wall cases and $(x/a)^{-1.3}$ for the channel center cases. These decay rates are lower than the $(x/a)^{-2}$ behavior observed by Legendre et al. (2006). In all cases the streamwise velocity deficit along *x*-axis in a turbulent flow is lower than that in the corresponding laminar flow (not shown here). This is due to the enhanced mixing in the wake in the presence of ambient turbulence and the faster recovery towards freestream velocity. The

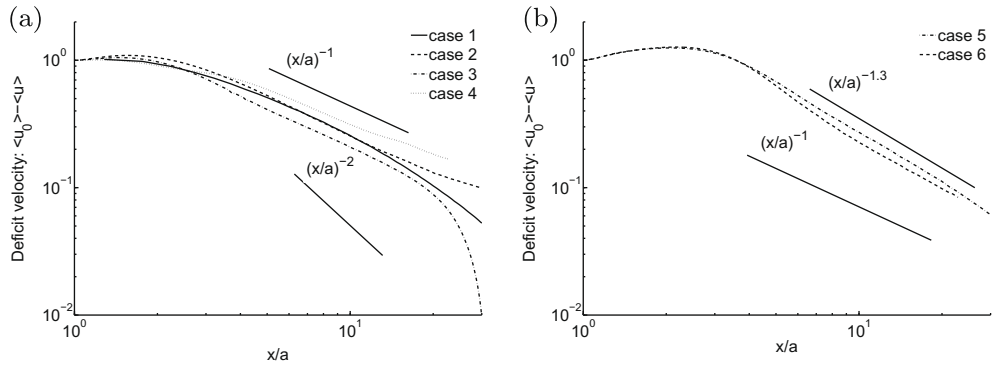

Fig. 3. Mean normalized streamwise velocity deficit along streamwise direction compared with the companion laminar flow. (a) Cases 1–4 ($y_{p+} = 17.81$). (b) Cases 5 and 6 ($y_{p+} = 178.12$).

effect is more significant at lower *Re* than at higher *Re*, since the wake for the higher *Re* is chaotic even in a laminar ambient flow.

To study the detailed mean wake shape, contours of zero streamwise velocity based on the time-averaged flow fields are plotted in Fig. 4. Also shown are the corresponding results for the laminar cases. It is seen that the recirculation region is shorter in the turbulent flow than that in the laminar flow, and the effect is more pronounced at high *Re*. This behavior is consistent with the finding for isotropic turbulence (Bagchi and Balachandar, 2004). The shorter recirculation region was attributed to the higher mixing in the particle wake in the presence of ambient turbulence. Other than the shorter recirculation region, we notice the obvious difference that the wakes in the buffer region (cases 1–4) with increasing particle Reynolds number tilts away from the wall.

Fig. 4a shows the contour of $\langle u \rangle = 0$ for case 1 ($d_+ = 3.56$, $y_{p+} = 17.81$, $Re = 42$). The contour is nearly symmetric about the particle centerline and the wake is almost the same as that in the laminar flow. For this case y_p/d is 5, and the wall has a negligible effect on the particle. This is consistent with observations in the context of a spherical particle settling parallel to a vertical wall in a quiescent ambient fluid that the wall has little effect on particle motion for $y_p/d \geqslant 4$ (Zeng et al., 2005, 2008). Therefore, in case 1 we can consider the particle to be sufficiently far away from the wall. Also due to the small particle Reynolds number, the mean wake is nearly axisymmetric in nature.

As the particle size increases (correspondingly the gap between the particle and the wall decreases), from Fig. 4b to d, the mean wake starts to tilt away from the wall in the turbulent cases. This is in contrast to what is observed in the companion laminar flow cases, where the wake is observed to tilt towards the wall. Again, in the context of a spherical particle settling parallel to a vertical wall it has been reported that the wall induces an *imperfect bifurcation* resulting in the formation of a double threaded wake (Zeng et al., 2005, 2009). The circulation of the streamwise-oriented vortex threads is such that their induced motion pushes them towards the wall, contributing to the downward tilt of the laminar wake. However, in the turbulent cases, both the mean shear and the ambient turbulence have a stronger effect. Perhaps in this case the reduced pressure due to the higher velocity above the particle, away from the bottom wall, contributes to upward tilting of the mean wake. The details of the lift force for the different turbulent cases have been discussed in detail in Zeng et al. (2008). Unlike in the laminar flow where the lift force on the particle is large and directed away from the wall (Zeng et al., 2005, 2009), in the turbulent flow it was observed that the mean lift force is negative and directed towards the wall. It is likely that the difference in the orientation of the mean wake contributes to this change in lift behavior (see Bagchi and Balachandar, 2002a,b).

For the channel center cases, contours of zero mean streamwise velocity are presented in Fig. 4e and f. In both these cases, the contours of side and top views are nearly identical. This reflects the near-isotropic nature of the wake at the channel center. Therefore, in later discussion of the channel center cases, only the top view will be used to illustrate the features of the wake. It is seen that in the turbulent flow the wake region is only slightly smaller than that in the laminar flow. This is because the particle Reynolds number in cases 5 and 6 is sufficiently large that natural vortex shedding and chaotic fluctuations are present in the wake even in the case of laminar ambient flow. Furthermore, the relative turbulent fluctuation in the incoming turbulent channel flow is only about 4% at the channel center.

3.2. Time-dependent wake

The time dependent nature of the particle wake is illustrated in Fig. 5 where contours of zero streamwise velocity are plotted for the buffer region cases (cases 1–4). The thick solid line represents the contour of mean zero streamwise velocity obtained from the time-averaged flow and the thin lines are the contours at various time instants. It is clear from the figure that the effect of incoming turbulence makes the particle wake unsteady in all the cases.

Fig. 5a and b corresponds to the two smaller particles. The mean Reynolds number for these cases is sufficiently small that the wake primarily responds to the unsteadiness of the ambient flow. The particle over time is subjected to increased (or decreased) streamwise flow during periods when a high (or low) speed streak is located at the particle location. Correspondingly the particle wake can be observed to shrink and grow episodically over time. However the general shape can be observed to remain the same. Figs. 6 and 7 show the vortical structures for case 1 ($d_+ = 3.56$, $y_{p+} = 17.81$, $Re = 42$) and case 2 ($d_+ = 10.69$, $y_{p+} = 17.81$, $Re = 125$) at two time instants. Here the vortical structure is identified in terms of an isosurface of swirling strength, defined as the imaginary part of the complex eigen pair of the local velocity gradient tensor. The suitability of this quantity for identifying coherent vortical structures has been discussed in Zhou et al. (1999) and Chakraborty et al. (2005). In case 2 occasionally a double-threaded wake appears, and the shape of the wake (oscillating back and forth) changes in response to the unsteadiness of the turbulent flow. However, since the particle Reynolds number is low for case 1, a double-threaded wake is not observed (see Fig. 6).

For the larger particles (Fig. 5c and d, cases 3 and 4), the vortex structures substantially change over time, especially for case 4. In Fig. 5d (case 4), the shape of the wake as given in the top and side views tilts to the right-upper corner and substantially departs from the mean. This suggests that the wake of the larger particle does not merely respond to changes in the incoming turbulent flow, but also include self-generated vortex shedding. The three-dimensional vortical structure for case 4 ($d_+ = 24.94$, $y_{p+} = 17.81$, $Re = 295$) is shown in Fig. 9 at two different time instants. For case 3, occasional vortex shedding is induced as the particle Reynolds number in-

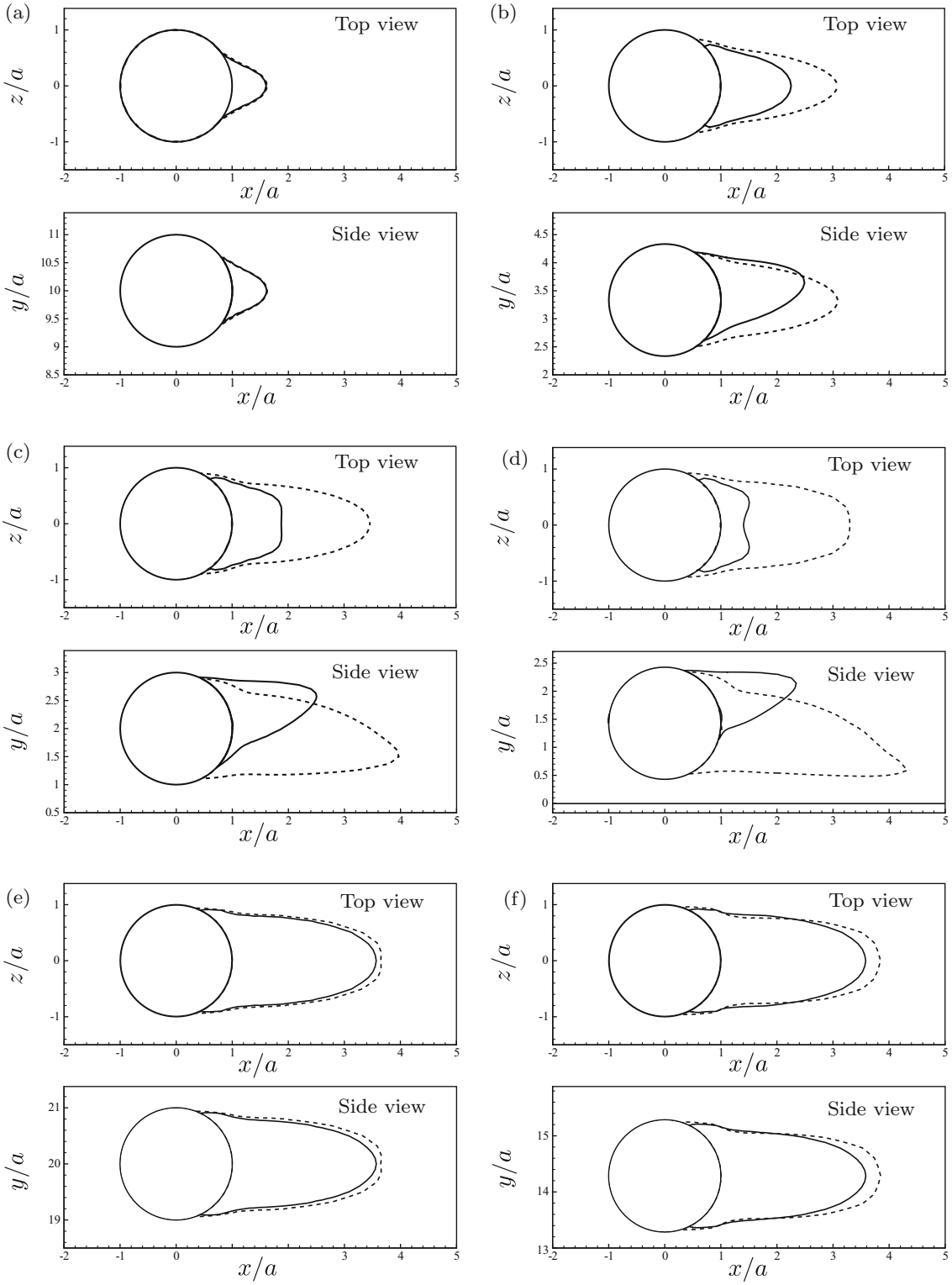

Fig. 4. Contours of zero streamwise velocity from the time-averaged mean flow fields in x–y and x–z planes. (a) Case 1, (b) case 2, (c) case 3, (d) case 4, (e) case 5, (f) case 6. —: Turbulent flow, - - -: laminar flow.

creases to larger value. As can be seen in Fig. 8 the wake appears to be more active at the time instant corresponding to frame (b) than at frame (a). The three-dimensional vortex structures for cases 5 and 6 are shown in Fig. 10. The structures exhibit unsteady vortex shedding. From the time history of the lift force (presented in Zeng et al. (2008)) an approximate shedding frequency can be computed. Due to the chaotic nature of force evolution it is hard to get a precise shedding frequency. Nevertheless we observe that the Strouhal number for the turbulent cases ranges from about 0.06 to 0.09, substantially lower than the corresponding laminar non-dimensional shedding frequency of about 0.15.

3.3. Turbulence modulation

In the present context of inflow–outflow turbulent channel-flow simulations with an embedded particle, the question of turbu-

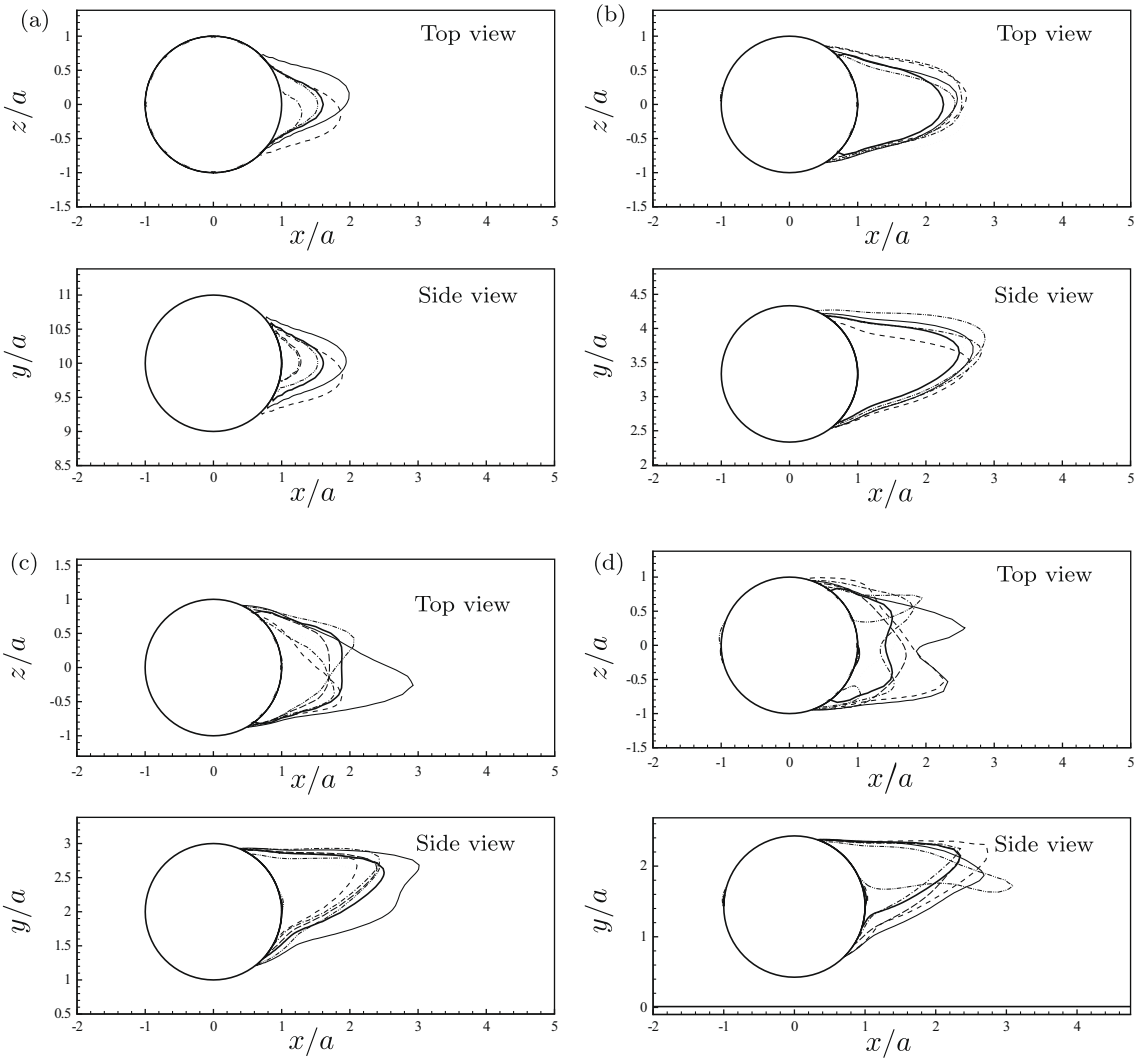

Fig. 5. Contours of zero streamwise velocity in x–y and x–z planes. (a) Case 1 ($d_+ = 3.56,\ y_{p+} = 17.81,\ Re = 42$). (b) Case 2 ($d_+ = 10.69,\ y_{p+} = 17.81,\ Re = 125$). (c) Case 3 ($d_+ = 17.81,\ y_{p+} = 17.81,\ Re = 210$). (d) Case 4 ($d_+ = 24.94,\ y_{p+} = 17.81,\ Re = 295$). Thick lines are based on time-averaged velocity. Thin lines are instantaneous contours at different time instants.

lence modulation by the particles can be indirectly addressed by focusing attention to the turbulence statistics in the wake region. Fig. 11 shows wall-normal profiles of mean streamwise velocity and rms turbulent velocity fluctuations at different distances downstream of the particle ($x/a = 2,\ 5$ and 10) for case 4. Also shown are the corresponding profiles for the turbulent channel flow without the particle (solid line). Note that in the later case the statistics are independent of the streamwise direction. Here $y = -1$ corresponds to the bottom wall and $y = 0$ corresponds to channel center and the particle is located at $y = -0.9$. It is interesting to note that the largest deficit is slightly above the particle, which corresponds to the upward tilt of the wake. In all cases it can be seen that for $y > -0.6$ the profiles are nearly independent of the streamwise location. However, deviation from the pure

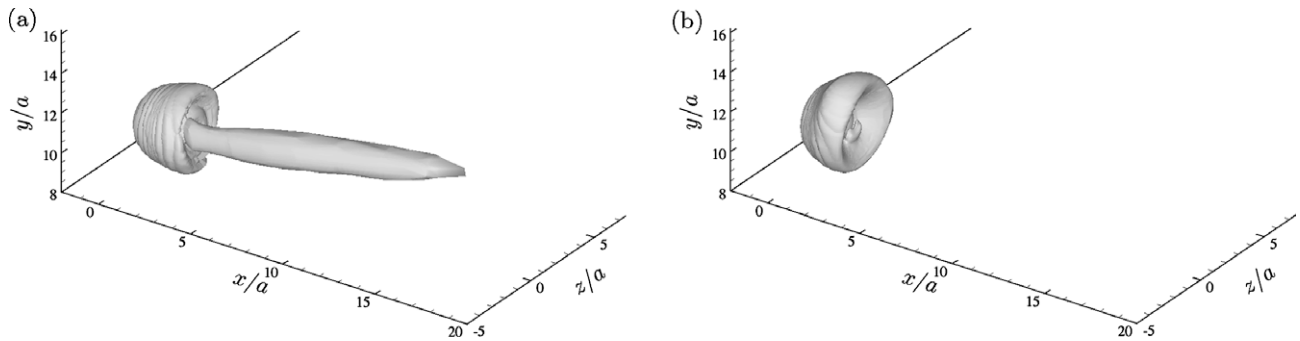

Fig. 6. Three-dimensional vortical structure with $\lambda_{ci} = 2.5$ for case 1 ($d_+ = 3.56,\ y_{p+} = 17.81,\ Re = 42$). (a) and (b) are for two time instants.

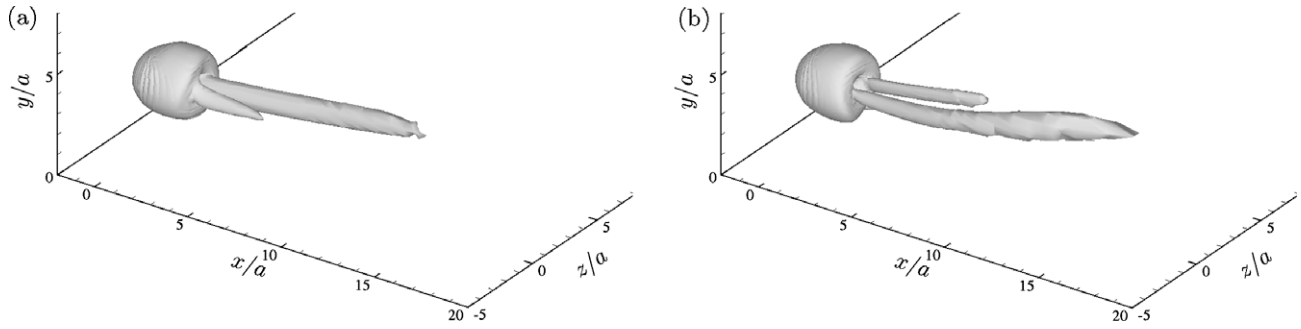

Fig. 7. Three-dimensional vortical structure with $\lambda_{ci} = 2.5$ for case 2 ($d_+ = 10.69,\ y_{p+} = 17.81,\ Re = 125$). (a) and (b) are for two time instants.

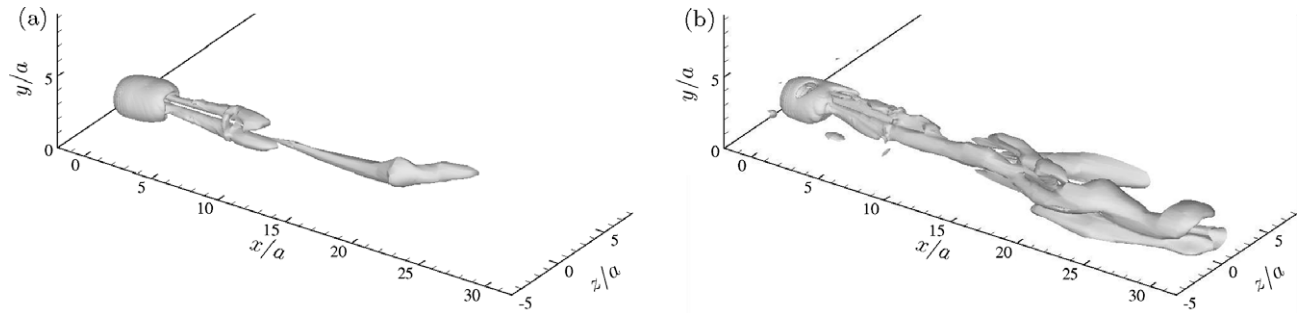

Fig. 8. Three-dimensional vortical structure with $\lambda_{ci} = 2.5$ for case 3 ($d_+ = 17.81,\ y_{p+} = 17.81,\ Re = 210$). (a) and (b) are for two time instants.

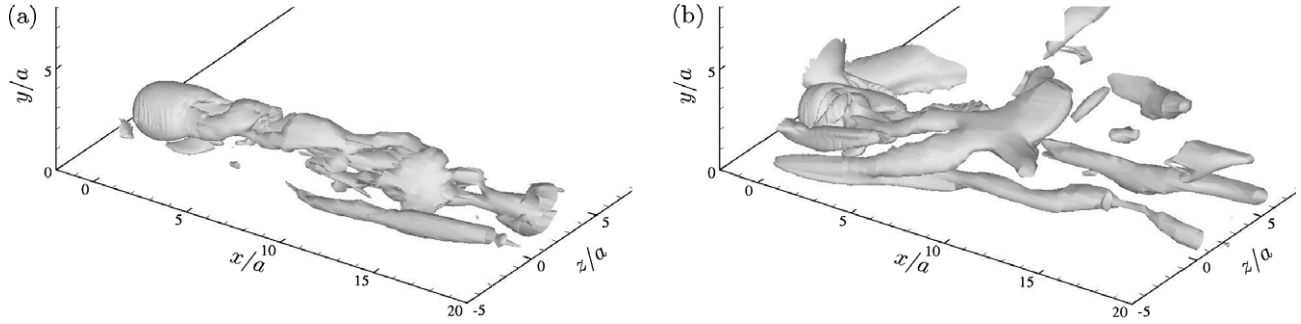

Fig. 9. Three-dimensional vortical structure with $\lambda_{ci} = 2.5$ for case 4 ($d_+ = 24.94,\ y_{p+} = 17.81,\ Re = 295$). (a) and (b) are for two time instants.

channel statistics persists far downstream. The behavior of cases 1–3 is similar. The only important difference is that as the particle size decreases its effect decays faster and the mean and rms statistics more rapidly approach those of pure channel. Also, from the mean velocity profiles, it can be seen that the shear stress at the bottom wall is significantly reduced over an extended region downstream of the particle. This has clear implication on drag modification.

We study the change in the total kinetic energy Ke_t and the fluctuation kinetic energy Ke_f due to the presence of the particle in the turbulent channel flow. Here the total kinetic energy Ke_t is defined as

$$Ke_t = \frac{1}{2}\langle \mathbf{u} \cdot \mathbf{u} \rangle \tag{1}$$

where $\mathbf{u}$ is the fluid velocity and $\langle\rangle$ indicates an average over time. The total kinetic energy will be scaled by a similarly defined total kinetic energy of the turbulent channel flow without the particle presence, Ke_t^0,

$$Ke_t^0 = \frac{1}{2}\langle\langle \mathbf{u}_0 \cdot \mathbf{u}_0 \rangle\rangle \tag{2}$$

where $\mathbf{u}_0$ is the undisturbed fluid velocity and $\langle\langle\rangle\rangle$ indicates an average over time, streamwise and spanwise directions.

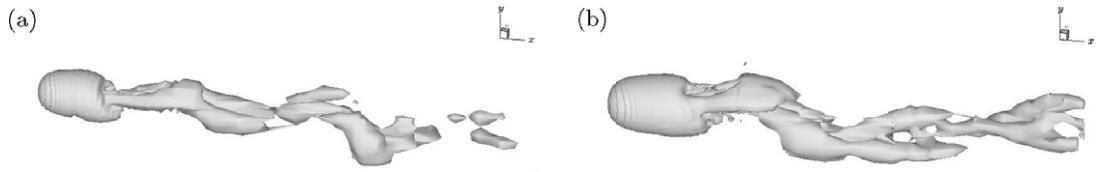

Fig. 10. Three-dimensional vortical structure with $\lambda_{ci} = 2.5$. (a) Case 5 ($d_+ = 17.81,\ y_{p+} = 178.12,\ Re = 325$). (b) Case 6 ($d_+ = 24.94,\ y_{p+} = 178.12,\ Re = 455$).

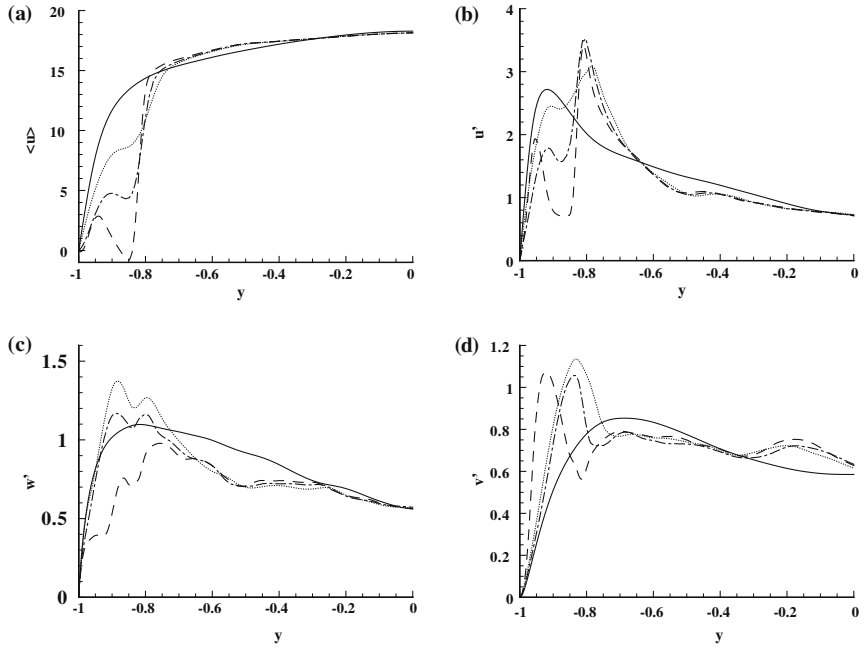

Fig. 11. Wall-normal profiles at different streamwise locations behind the particle for case 4. - - - - : $x/a = 2$; — · — · — : $x/a = 5$; ⋯ : $x/a = 10$; solid Line: channel flow statistics without the particle. (a) Mean streamwise velocity, (b) rms streamwise velocity fluctuation, (c) rms spanwise velocity fluctuation, (d) rms wall-normal fluctuation.

3.3.1. Total kinetic energy

The variation of total kinetic energy along the *x*-axis in the particle wake is shown in Fig. 12. Fig. 12a presents the results for the buffer region cases 1–4. It is clear in all the cases considered the recovery of the total kinetic energy in the wake is less than 80% even 20 radii downstream of the sphere and thus the particle has a sustained effect that extends far downstream. Case 2 shows the slowest recovery, substantially lower than case 1. In both these cases the wall effect is not strong and as a result the wake is relatively horizontal without much tilt. The effect of increasing Reynolds number in this range is to extend the wake and slow the recovery to freestream values.

Compared to case 2, the recovery of total kinetic energy appears to be more rapid in cases 3 and 4. As seen in Fig. 4c the primary reason is the upward tilting of the wake for these larger particles. In these cases the largest reduction in the total kinetic energy is not directly behind the sphere center, and as a result along the horizontal line through the particle center the total kinetic energy appears to recover faster. Turbulence induced vortex shedding also plays an important role. For case 3 vortex shedding is occasional and occurs only when the instantaneous Reynolds number increases to larger values. Whereas in case 4, where the mean Reynolds number is sufficiently large, wake vortex shedding is sustained. In the case of the largest particle (case 4) the gap between the particle and the bottom wall is limited (in wall units the gap is 5.34) and the asymmetry introduced by the wall is the strongest. Vortex shedding is predominantly one-sided and occurs only farther away from the wall on the top side of the particle, while shedding at the bottom is inhibited by the wall. The effect of vortex shedding is to slow the approach of the total kinetic energy to undisturbed value. In fact, the non-monotonic behavior in Ke_t/Ke_t^0 is indicative of strong vortex shedding and can be observed for the two cases of particle placed at the channel center as well. For cases 5 and 6, shown in Fig. 12b, particle Reynolds number is high and sustained vortex shedding is observed. For the larger particle, due to the increased Reynolds number the wake energy recovers at a slightly more rapid rate.

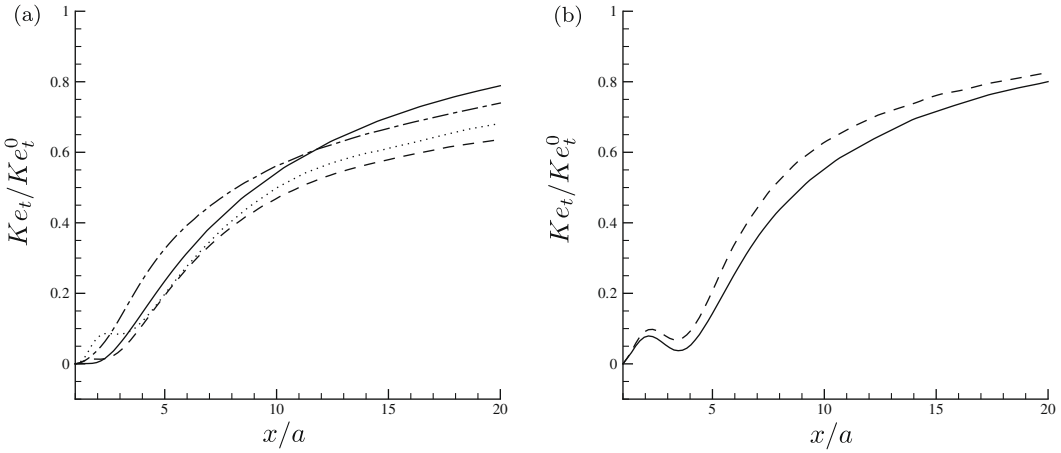

Fig. 12. Total kinetic energy Ke_t/Ke_t^0 distribution along *x*-axis. (a) At buffer region $y_{p+} = 17.81$. —: Case 1, - - - : case 2, — · —: case 3, ⋯: case 4. (b) At channel center $y_{p+} = 178.12$. —: Case 5, - - -: case 6.

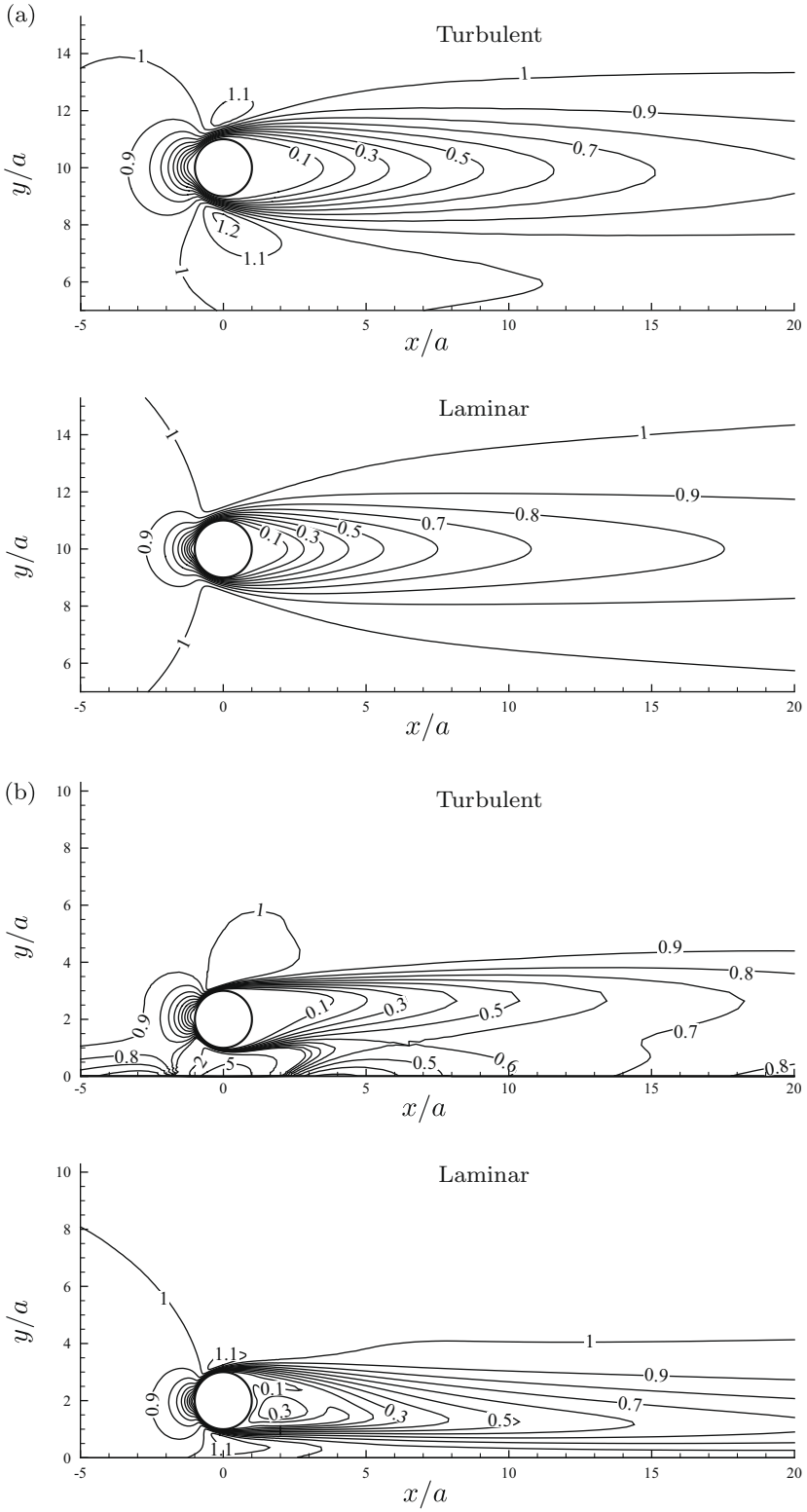

Fig. 13. Total kinetic energy Ke_t/Ke_t^0 compared with the companion laminar simulation for (a) case 1 ($d_+ = 3.56$, $y_{p+} = 17.81$, $Re = 42$) and (b) case 3 ($d_+ = 17.81$, $y_{p+} = 17.81$, $Re = 210$). Here both are side views.

Fig. 13 shows the contour plots of the total kinetic energy for cases 1 and 3 plotted on the x–y (vertical) plane passing through the particle center. Also plotted for comparison are the corresponding results for the laminar flow cases. The total kinetic energy in the turbulent flow recovers faster than in the laminar ambient. Such effect is more pronounced for the larger particle. For the smallest particle (case 1), the total kinetic energy remains nearly symmetric even on the y–z plane suggesting the influence of the wall to be insignificant. At this low Reynolds number ($Re = 42$) there is no vortex shedding in either the turbulent channel flow or the corresponding

laminar flow. In the case of turbulent flow, the wake oscillates in response to fluctuations in the incoming flow. This wake oscillation contributes to the somewhat faster recovery.

The behavior of the total kinetic energy is consistent with our discussion of the mean wake length. In case 3, the recovery of total kinetic energy to undisturbed values is more rapid in the turbulent flow. For this case the mean Reynolds number ($Re = 210$) is still small that there is no vortex shedding for the laminar inflow. With turbulent inflow the wake oscillates in response to inflow fluctuation, and occasionally as the particle Reynolds number based on instantaneous relative velocity increases above a threshold, vortex shedding is observed. Together the two mechanisms contribute to the enhanced wake recovery. Note that in a uniform ambient flow the critical *Re* for vortex shedding is around 280 (Natarajan and Acrivos, 1993). Also note that as in the shape of the mean wake, the total kinetic energy contours for the laminar flow are tilted down towards the wall, while they are tilted away from the wall for the turbulent flow.

3.3.2. Fluctuation kinetic energy

Total kinetic energy can be divided into two key contributions, one from the time-averaged mean flow and the other from fluctuations. The contribution from fluctuations is of great interest in order to understand how turbulence fluctuations are modulated by the particle. The fluctuation kinetic energies Ke_f and Ke_f^0 are defined as

$$Ke_f = \frac{1}{2}\langle|\mathbf{u} - \langle\mathbf{u}\rangle|^2\rangle \tag{3}$$

$$Ke_f^0 = \frac{1}{2}\langle\langle|\mathbf{u}_0 - \langle\langle\mathbf{u}_0\rangle\rangle|^2\rangle\rangle \tag{4}$$

where again $\mathbf{u}$ and $\mathbf{u}_0$ are the velocity with and without the particle. Fig. 14 shows contours of fluctuation kinetic energy in the vicinity of the particle on both the *x*–*z* and *x*–*y* planes for the four cases of particle in the buffer region. For the smallest particle (case 1) the effect of the particle is to reduce turbulent fluctuation. As with the

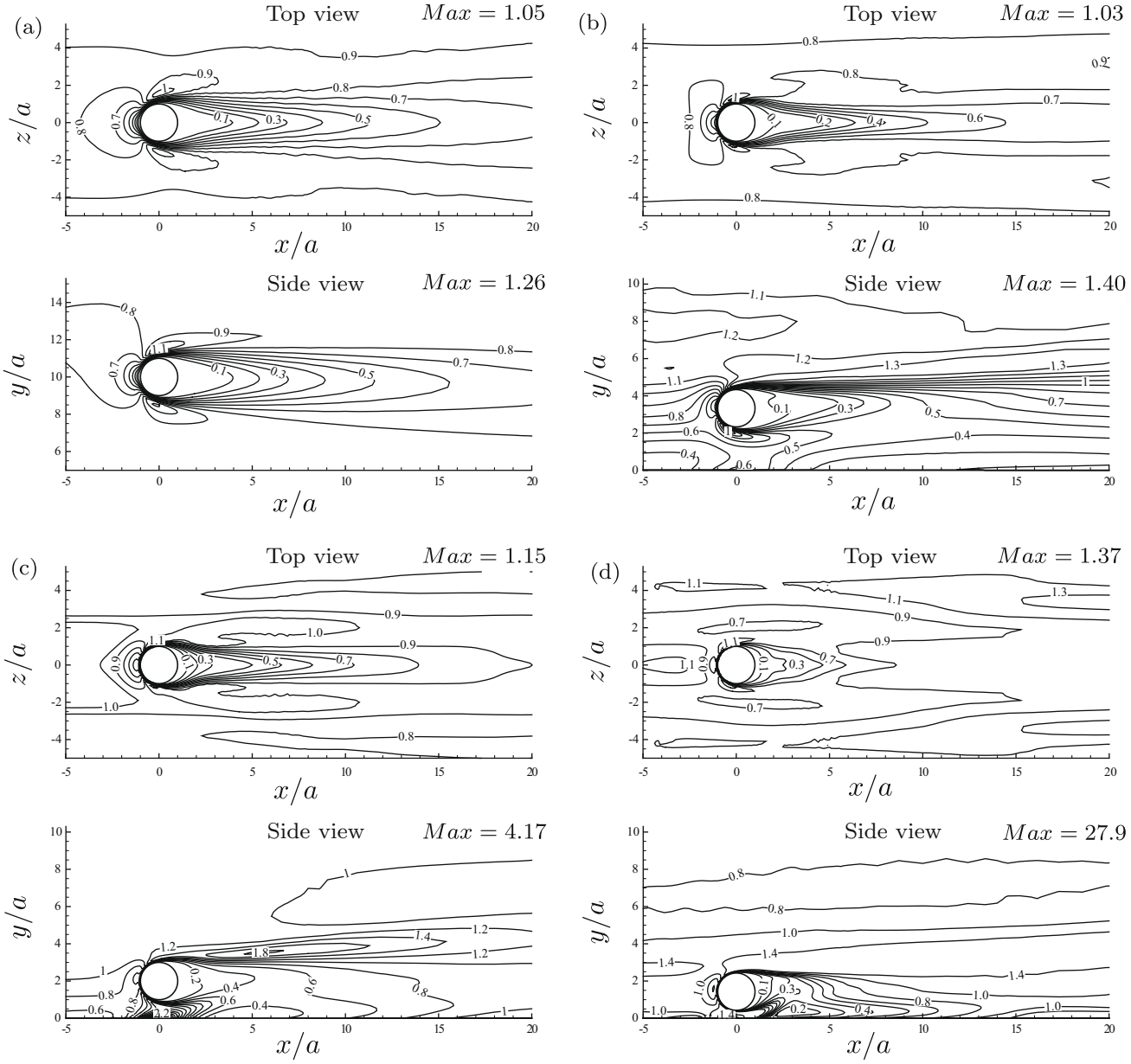

Fig. 14. Fluctuation kinetic energy Ke_f/Ke_f^0 in the $y_+ = 17.81$ plane for buffer region cases. (a) Case 1, (b) case 2, (c) case 3, (d) case 4.

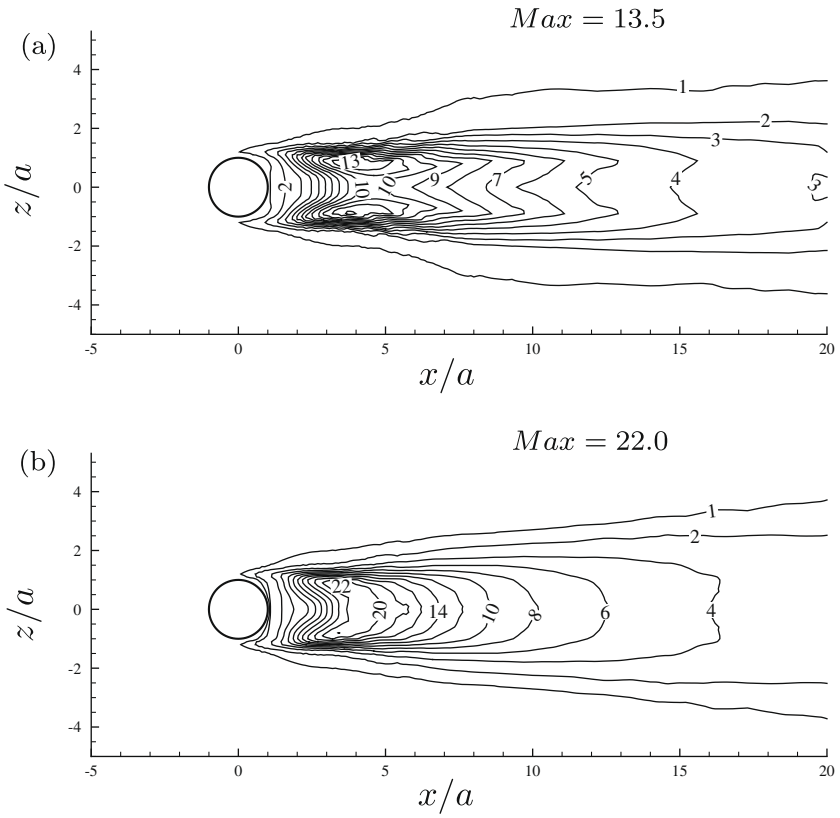

Fig. 15. Fluctuation kinetic energy Ke_f/Ke_f^0 in the $y_+ = 178.12$ plane for channel center cases. (a) Case 5 and (b) case 6.

mean wake and total kinetic energy, the reduction in turbulent kinetic energy (TKE) extends several diameters downstream of the particle and recovery is only about 70% complete even at 10 diameters downstream. On the horizontal x–z plane turbulence suppression extends over a wide region along the spanwise direction. On the vertical x–y plane, the wake can be seen to be slightly tilted down towards the wall. Only over a very small region directly above the particle TKE is slightly enhanced. Thus, small particles placed within the buffer region contribute to suppression of turbulence.

The results for case 2 are qualitatively similar to case 1, although recovery to freestream fluctuation levels is more rapid along the streamwise direction. The influence of the particle extends over a wider region along the spanwise direction. On the vertical plane, turbulent kinetic energy is enhanced over a larger region located above the particle.

For cases 3 and 4 we can observe the increase in Ke_f on both the x–z and x–y planes. The regions of substantial increase in these cases suggest vortex shedding and shear layer instability to the top and

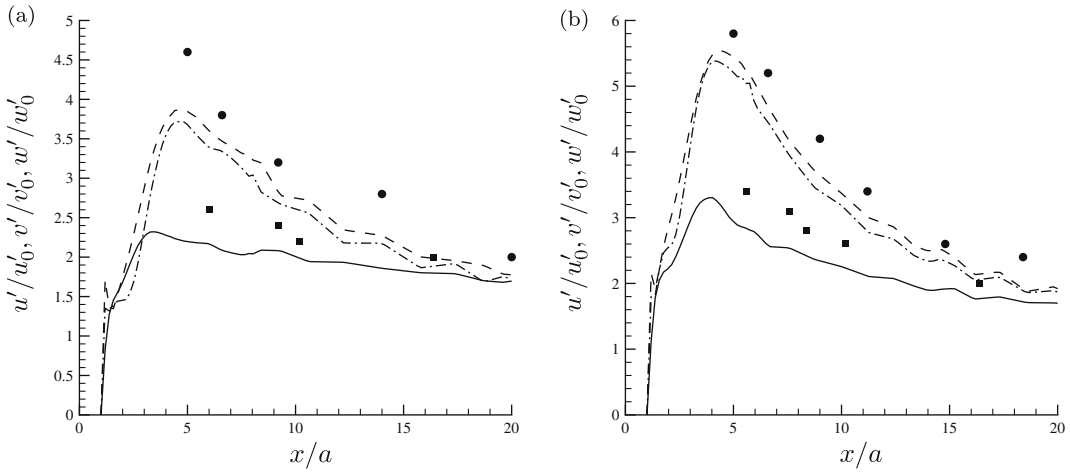

Fig. 16. Comparison of the rms velocities with the experimental results of Wu and Faeth (1994a). (a) Case 5 ($d/\eta = 4.8$, $\langle \mathrm{Re}_r \rangle = 325$, $I = 4.09\%$) compared with data of Wu and Faeth (1994a) with $d/\eta = 3.7$, $\langle \mathrm{Re}_r \rangle = 300$, $I = 4.2\%$. (b) Case 6 ($d/\eta = 6.7$, $\langle \mathrm{Re}_r \rangle = 455$, $I = 4.09\%$) compared with data of Wu and Faeth (1994a) with $d/\eta = 4.8$, $\langle \mathrm{Re}_r \rangle = 415$, $I = 3.9\%$. ——: Present, streamwise, - - -: present, wall-normal, — · —: present, spanwise. ■: Wu and Faeth (1994a), streamwise, •: Wu and Faeth (1994a), cross-stream.

the sides of the particle. In both these cases the suppression of turbulence in the wake recovers much more rapidly along the downstream direction. In the x–y plane, although the maximum value of Ke_f/Ke_f^0 is very high (for example, in case 4 it reaches 28) we notice it occurs only in the gap between the particle and the bottom wall around $y_+ = 0.12$ (just above the wall). Note that normalization Ke_f^0 is based on local undisturbed values. Thus, for the largest particle the lower levels of turbulence in the viscous sublayer are substantially enhanced under the particle. Also note that in all these figures the coordinates are scale by particle radius. Thus, the domain of turbulence enhancement seen in case 2 is much smaller than for the larger particles.

Fig. 15 shows the fluctuation kinetic energy in the vicinity of the particle for the two cases (5 and 6), where the particle is located at the channel center. There is a fundamental difference between these results and those shown in Fig. 14 for the buffer region. Turbulence enhancement is substantial and it extends over a wide region in the wake. It should be noted that for the case of particles in the buffer region the ratio of turbulence fluctuation in the incoming flow to the mean relative velocity is $I = 23.16\%$ and the corresponding ratio for the channel center is only $I = 4.09\%$. Thus the relative level of ambient turbulence at the channel center is much weaker than in the buffer region. As pointed out by Bagchi and Balachandar (2004), at lower levels of freestream turbulence, the fluctuation kinetic energy shows substantial enhancement in the wake, indicating local augmentation of turbulence. This enhancement is mostly due to vortex shedding. They observed the maximum value for Ke_f/Ke_f^0 in the wake for $I = 10\%$, $Re = 610$ to be as high as 17.8. In the present case 6 at $Re = 455$ we have an even lower turbulence intensity ($I = 4.09\%$) and we get quite large augmentation by as much as factor 22. Thus, in agreement with the finding of Bagchi and Balachandar (2004), at lower level of freestream turbulence and a large particle, vortex shedding contributes to significant enhancement of the fluctuation kinetic energy in the

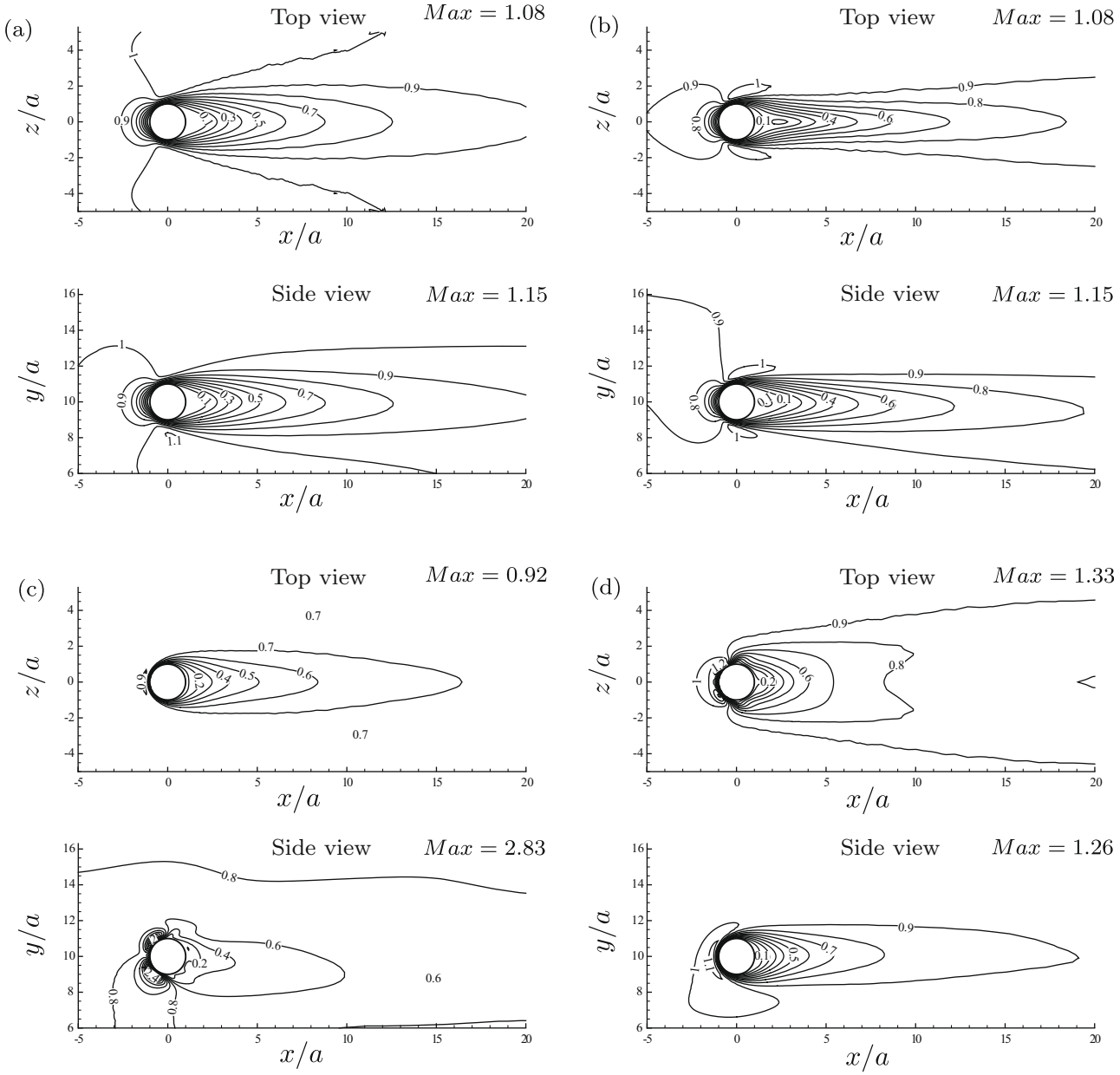

Fig. 17. Velocity distributions for case 1 ($d_+ = 3.56$, $y_{p+} = 17.81$, $Re = 42$). (a) Mean streamwise velocity $\langle u\rangle/\langle u_0\rangle$, (b) rms streamwise velocity u'/u'_0, (c) rms wall-normal velocity v'/v'_0, (d) rms spanwise velocity w'/w'_0.

particle wake. In contrast, for the buffer region cases, the fluctuation kinetic energy is suppressed or only marginally increased. This indicates that at a higher level of ambient turbulence, wake oscillation or even vortex shedding does not result in significant enhancement of the fluctuation kinetic energy. In isotropic turbulence, Bagchi and Balachandar (2004) observed the wake oscillation to result in substantial contribution to fluctuation only at lower levels of ambient turbulence.

In a turbulent channel the statistics of the streamwise, wall-normal and spanwise components of velocity are different and the difference is significant as the walls are approached. However, the statistics tends towards isotropy near the channel center. In recognition of the non-isotropy of the turbulence statistics, here we consider the three components of fluctuating velocity separately. The rms velocity fluctuations are defined as

$$u' = \sqrt{\langle (u - \langle u \rangle)^2 \rangle}, \quad v' = \sqrt{\langle (v - \langle v \rangle)^2 \rangle},$$
$$w' = \sqrt{\langle (w - \langle w \rangle)^2 \rangle} \tag{5}$$

Similarly, the 'undisturbed' rms velocity fluctuations are

$$u'_0 = \sqrt{\langle \langle (u_0 - \langle \langle u_0 \rangle \rangle)^2 \rangle \rangle}, \quad v'_0 = \sqrt{\langle \langle (v_0 - \langle \langle v_0 \rangle \rangle)^2 \rangle \rangle},$$
$$w'_0 = \sqrt{\langle \langle (w_0 - \langle \langle w_0 \rangle \rangle)^2 \rangle \rangle} \tag{6}$$

We use the scaled rms velocities (u'/u'_0, v'/v'_0, w'/w'_0) to address the effect of the particle on turbulence.

Fig. 16a shows a comparison of rms velocity fluctuations for case 5 along the sphere centerline with the experiment results of Wu and Faeth (1994a). They considered a stationary particle subjected to a turbulent pipe flow of intensity $I = 4\%$. The present results are in good qualitative agreement with their measurements, while quantitatively the present results for the streamwise and cross-stream velocity components are somewhat lower. The smaller values may be due to the stronger influence of the walls, which tend to suppress turbulence, especially as the particle size becomes large compared to the gap.

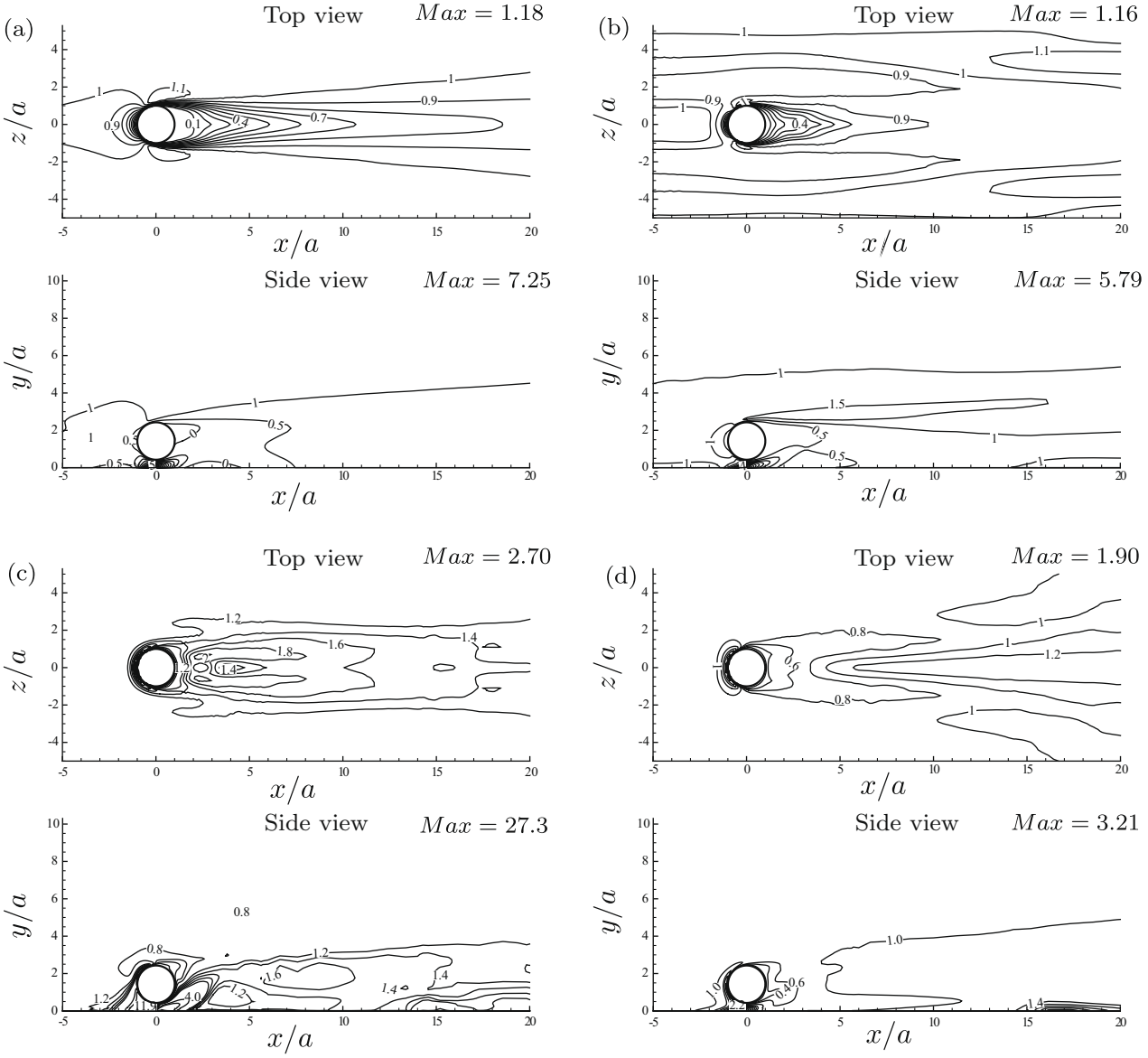

Fig. 18. Velocity distributions for case 4 ($d_+ = 24.94$, $y_{p+} = 17.81$, $Re = 295$). (a) Mean streamwise velocity $\langle u \rangle / \langle u_0 \rangle$, (b) rms streamwise velocity u'/u'_0, (c) rms wall-normal velocity v'/v'_0, (d) rms spanwise velocity w'/w'_0.

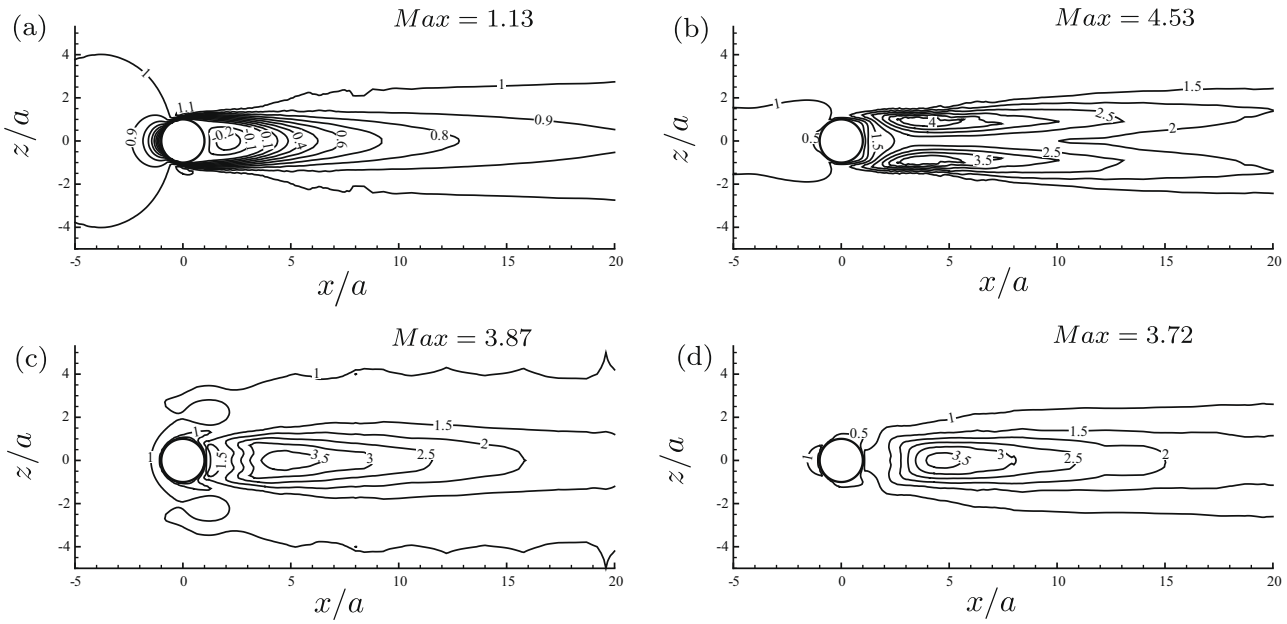

Fig. 19. Velocity distributions for case 5 ($d_+ = 17.81,\ y_{p+} = 178.12,\ Re = 325$). (a) Mean streamwise velocity $\langle u\rangle/\langle u_0\rangle$, (b) rms streamwise velocity u'/u'_0, (c) rms wall-normal velocity v'/v'_0, (d) rms spanwise velocity w'/w'_0.

Figs. 17 and 18 show the scaled velocity distributions for cases 1 and 4. For case 1, shown in Fig. 17, the rms fluctuations of all three velocity components are in general damped in the wake region. There is a small region located near the front stagnation point where the vertical velocity fluctuations, and to a lesser extent spanwise velocity fluctuations, are augmented. This enhancement can be explained in terms of the rapid distortion of the incoming turbulence as it flows around the sphere, where the streamwise fluctuations are suppressed at the expense of the other two components. The overall effect of the particle is to dampen turbulence. For case 2 (not shown here) the velocity distribution is similar, and the streamwise and wall-normal components (u'/u'_0 and v'/v'_0) show an increase, but again primarily around the stagnation region in front of the particle.16

Cases 3 and 4 are different from cases 1 and 2. In addition to the increase in the level of wall-normal and spanwise velocity fluctuations arising from the rapid distortion of turbulence ahead of the particle, significant regions of turbulence enhancement can be seen in the wake, especially in the shear layer regions above the particle away from the wall. The increase of fluctuation kinetic energy mainly comes from the wall-normal component, v'/v'_0, and primarily due to vortex shedding. Sustained one-sided vortex shedding above the sphere dominantly affects the wall-normal component.

Fig. 19 shows detailed mean and rms velocity distributions in the particle wake for case 5 ($d_+ = 17.81,\ y_{p+} = 178.12,\ Re = 325$). The rms fluctuations in all three velocity components ($u',\ v',\ w'$) increase by a large amount, which results in significant augmentation of the fluctuation kinetic energy. The contours of wall-normal and spanwise components ($v'/v'_0,\ w'/w'_0$) are nearly identical, which is due to the near isotropy of the incoming turbulence at the channel center. Also the scaled rms fluctuations on the x–y plane are similar and therefore not shown here. The same behavior applies to the larger particle (case 6) with an even larger enhancement (not shown here). The peak values of streamwise velocity ratio and scaled fluctuations are shown in Table 3.

Table 3
Peak values of scaled mean streamwise velocity and turbulence velocity fluctuations.

Case	Top view (x–z plane)				Side view (x–y plane)			
	$\langle u\rangle/\langle u_0\rangle$	u'/u'_0	v'/v'_0	w'/w'_0	$\langle u\rangle/\langle u_0\rangle$	u'/u'_0	v'/v'_0	w'/w'_0
1	1.08	1.08	0.92	1.33	1.15	1.15	2.83	1.26
2	1.03	1.03	1.94	1.54	1.45	1.25	4.05	1.39
3	1.15	1.08	2.35	1.72	3.57	2.11	11.1	1.81
4	1.18	1.16	2.70	1.90	7.25	5.79	27.3	3.21
5	1.13	4.53	3.87	3.72				
6	1.12	5.80	5.54	5.40				

3.4. Wall shear stress

In this section, we address the change in wall shear stress with the presence of a particle in the turbulent channel flow. The wall shear stress τ_w is defined as

$$\tau_w = \mu\left\langle\frac{\partial u}{\partial y}\right\rangle \tag{7}$$

Similarly τ_w^0 is the undisturbed wall shear stress defined as

$$\tau_w^0 = \mu\left\langle\frac{\partial u_0}{\partial y}\right\rangle \tag{8}$$

For cases where the particle is located in the buffer region, the scaled wall shear stress is shown in Fig. 20. For a particle at the channel center, the influence on wall shear stress is minimal, since the particle is far away from the wall.

Fig. 20a shows the smallest particle, which can be considered to be sufficiently far away from the wall. The particle has a negligible effect on wall shear stress as expected. As the particle becomes larger and the gap decreases, the effect is more substantial. The maximum wall shear stress occurs right below the particle. For the largest particle (case 4), the maximum value of the ratio is as high as 8.11. Interestingly, we notice that there's a wake-like region downstream of the particle in cases 3 and 4, where wall shear stress is reduced. As particle becomes larger, the region of shear stress enhancement (region enclosed by contour level 1) relative to the particle size is more concentrated. However note that in this figure the streamwise and spanwise distances are scaled by particle radius and thus with increasing particle size a larger platform of enhanced wall shear stress is realized.

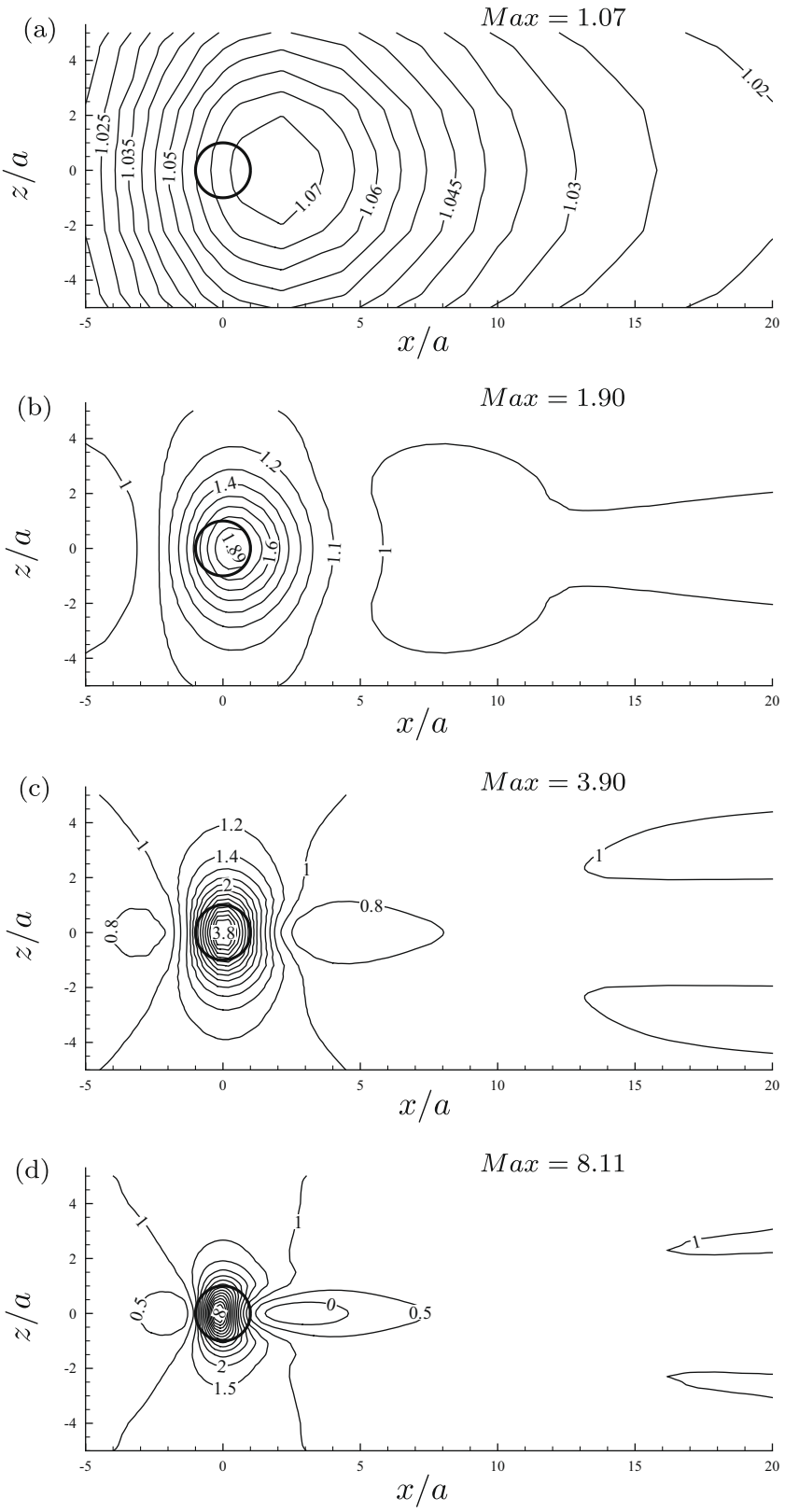

Fig. 20. Wall shear stress τ_w/τ_w^0 distribution on the bottom wall for the buffer region cases. (a) Case 1, (b) case 2, (c) case 3, (d) case 4.

4. Conclusions

Here we consider a finite-sized particle in a turbulent channel flow with $Re_\tau = 178.12$. The particle Reynolds number ranges from about 40 to 450, and the location of the particle is chosen to be either in the buffer layer ($y_{p+} = 17.81$) or at the channel center. The ambient turbulence intensity relative to mean velocity is large ($I = 23.16\%$) in the buffer region, while it is substantialy lower

($I = 4.09\%$) at the channel center. The purpose of this paper is to present the effect of the particle wake dynamics and vortex shedding on turbulence modulation. The major conclusions to be drawn are as follows:

- We observe the time-averaged mean mean wake length to reduce when the ambient flow is turbulent. The reduction is more pronounced with higher turbulence intensity and at larger particle Reynolds number. Particle wake is seen to tilt away from the wall. This is in contrast to particle moving parallel to a nearby wall in a stagnant fluid where the wake tilt is towards the wall. The wake length for a particle in a turbulent channel flow is in agreement with that for a particle in isotropic turbulence (Bagchi and Balachandar, 2004).
- Wake oscillation is observed in response to the unsteadiness of the ambient turbulence. For particles with $Re < 210$, oscillation is limited to the wake region. For $Re \approx 210$, occasional vortex shedding is induced when the particle Reynolds number increases to a larger value. For $Re > 210$ vortex shedding is mostly present. Vortex shedding plays a significant role in the enhancement of turbulent kinetic energy.
- The total kinetic energy is significantly reduced in the wake region. The energy of the wake region in turbulent flow recovers more rapidly than in laminar flow due to enhanced mixing. When particle size has not reached the threshold to induce vortex shedding, a larger particle reduces more energy in the wake region. When particle is large enough to induce vortex shedding, the chaotic process in the wake promotes faster recovery.
- The effect of particle on the turbulent kinetic energy is also studied in terms of the fluctuation kinetic energy. Two mechanisms are observed to enhance the fluctuation kinetic energy, i.e., vortex shedding and wake oscillation. Wake oscillation plays a less important roles in the presence of vortex shedding. At higher levels of turbulence (in the buffer region) the effect of small particles is observed to suppress turbulence, since wake oscillation is less effective to compensate for enhanced dissipation. Whereas large particles are observed to enhance turbulence mainly due to vortex shedding. At the channel center a much more substantial augmentation is observed.
- In the buffer region the increase in fluctuation kinetic energy is mainly in the wall-normal component. At the channel center the increase is almost equally partitioned among all three components.
- The maximum wall shear stress occurs right below the particle. For the cases with vortex shedding the contour of wall shear stress also shows a wake-like behavior. With increasing particle size, the enhancement region of wall shear stress relative to particle size becomes more concentrated close to the particle.

Acknowledgments

This research was supported by the ASCI Center for the Simulation of Advanced Rockets at the University of Illinois at Urbana-Champaign through the US Department of Energy (subcontract number B523819) and NSF CBET0639446. The National Center for Supercomputing Applications (UIUC) is also acknowledged, for the use of their computational facilities.

References

Bagchi, P., Balachandar, S., 2002b. Shear versus vortex-induced lift force on a rigid sphere at moderate Re. J. Fluid Mech. 473, 379–388.

Bagchi, P., Balachandar, S., 2002a. Effects of free rotation on the motion of a solid sphere in linear shear flow at moderate Re. Phys. Fluids 14, 2719–2737.

Bagchi, P., Balachandar, S., 2003. Effect of turbulence on the drag and lift of a particle. Phys. Fluids 15, 3496–3513.

Bagchi, P., Balachandar, S., 2004. Response of the wake of an isolated particle to an isotropic turbulent flow. J. Fluid Mech. 518, 95–123.

Burton, T.M., Eaton, J.K., 2005. Fully resolved simulations of particle–turbulence interaction. J. Fluid Mech. 545, 67–111.

Caraman, N., Boree, J., Simonin, O., 2003. Effect of collisions on the dispersed phase fluctuation in a dilute tube flow: experimental and theoretical analysis. Phys. Fluids 15, 3602–3612.

Chakraborty, P., Balachandar, S., Adrian, R.J., 2005. On the relationships between local vortex identification schemes. J. Fluid Mech. 535, 189–214.

Crowe, C.T., Sommerfeld, M., Tsuji, Y., 1998. Multiphase Flows with Droplets and Particles. CRC Press, New York.

Elghobashi, S., Truesdell, G.C., 1993. On the 2-way interaction between homogeneous turbulence and dispersed solid particles. 1: turbulence modification. Phys. Fluids 5, 1790–1801.

Fessler, J.R., Kulick, J.D., Eaton, J.K., 1994. Preferential concentration of heavy particles in a turbulent channel flow. Phys. Fluids 6, 3742–3749.

Hetsroni, G., 1989. Particles–turbulence interaction. Int. J. Multiphase Flow 15, 735–746.

Hwang, W., Eaton, J.K., 2006. Homogeneous and isotropic turbulence modulation by small heavy ($St \sim 50$) particles. J. Fluid Mech. 564, 361–393.

Johnson, T.A., Patel, V.C., 1999. Flow past a sphere up to a Reynolds number of 300. J. Fluid Mech. 378, 19–70.

Kaftori, D., Hetsroni, G., Banerjee, S., 1995a. Particle behavior in the turbulent boundary layer: I. Motion, deposition and entrainment. Phys. Fluids 7, 1095–1106.

Kaftori, D., Hetsroni, G., Banerjee, S., 1995b. Particle behavior in the turbulent boundary layer: II. Velocity and distribution profiles. Phys. Fluids 7, 1107–1121.

Kajishima, T., Takiguchi, S., Hamasaki, H., Miyake, Y., 2001. Turbulence structure of particle-laden flow in a vertical plane channel due to vortex shedding. JSME Int. J. Ser. B – Fluids Thermal Eng. 44, 526–535.

Legendre, D., Merle, A., Magnaudet, J., 2006. Wake of a spherical bubble or a solid sphere set fixed in a turbulent environment. Phys. Fluids 18, 048102.

Merle, A., Legendre, D., Magnaudet, J., 2005. Forces on a high-Reynolds-number spherical bubble in a turbulent flow. J. Fluid Mech. 532, 53–62.

Mittal, R., 2000. Response of the sphere wake to free-stream fluctuations. Theor. Comput. Fluid Dyn. 13, 397–419.

Natarajan, R., Acrivos, A., 1993. The instability of the steady flow past spheres and disks. J. Fluid Mech. 254, 323–344.

Pan, Y., Banerjee, S., 1997. Numerical investigations of the effects of large particles in wall turbulence. Phys. Fluids 9, 3786–3807.

Rashidi, M., Hetsroni, G., Banerjee, S., 1990. Particle turbulence interaction in a boundary layer. Int. J. Multiphase Flow 16, 935–949.

Rimon, Y., Cheng, S.I., 1969. Numerical simulations of a uniform flow over a sphere at intermediate Reynolds numbers. Phys. Fluids 12, 949–959.

Suzuki, Y., Ikenoya, M., Kasagi, N., 2000. Simultaneous measurement of fluid and dispersed phases in a particle-laden turbulent channel flow with the aid of 3-D PTV. Exp. Fluids 29, s185–s193.

Taneda, S., 1956. Studies on Wake Vortices (III). Experimental Investigation of the Wake Behind a Sphere at Low Reynolds Number. Rep. Res. Inst. Appl. Mech., Kyushu Univ. vol. 4, pp. 99–105.

Tsuji, Y., Morikawa, Y., Shiomi, H., 1984. LDV measurements of an air-solid two-phase flow in a vertical pipe. J. Fluid Mech. 139, 417–434.

Uhlmann, M., 2008. Interface-resolved direct numerical simulation of vertical particulate channel flow in the turbulent regime. Phys. Fluids 20, 053305.

Wu, J.S., Faeth, G.M., 1994a. Sphere wakes at moderate Reynolds numbers in a turbulent environment. AIAA J. 32, 535–541.

Wu, J.S., Faeth, G.M., 1994b. Effect of ambient turbulence intensity on sphere wakes at intermediate Reynolds numbers. AIAA J. 33, 171–173.

Young, J.B., Hanratty, T.J., 1991. Optical studies on the turbulent motion of solid particles in a pipe flow. J. Fluid Mech. 231, 665–688.

Zeng, L., Balachandar, S., Fischer, P., 2005. Wall-induced forces on a rigid sphere at finite Re. J. Fluid Mech. 536, 1–25.

Zeng, L., Balachandar, S., Fischer, P., Najjar, F., 2008. Interactions of a stationary finite-sized particle with wall turbulence. J. Fluid Mech. 594, 271–305.

Zeng, L., Najjar, F.M., Balachandar, S., Fischer, P., 2009. Forces on a finite-sized particle located close to a wall in a linear shear flow. Phys. Fluids 21, 033302.

Zhou, J., Adrian, R.J., Balachandar, S., Kendall, T.M., 1999. Mechanisms for generating coherent packets of hairpin vortices in channel flow. J. Fluid Mech. 387, 353–396.